LANGMUIR

pubs.acs.org/Langmuir Article

Nanoporous Thin Films Formed from Photocleavable Diblock Copolymers on Gold Substrates Modified with Thiolate Self-Assembled Monolayers

Takashi Ito,* Herman Coceancigh, Yi Yi,* Jay N. Sharma, Fred C. Parks, and Amar H. Flood

Cite This: *Langmuir* 2020, 36, 9259−9268 Read Online

ACCESS | Metrics & More | Article Recommendations | Supporting Information

ABSTRACT: Nanoporous thin films formed on electrodes are considered functional elements of electrochemical sensing systems, thus motivating methods for their development. We report a preparative strategy detailing the effects of surface modification of gold substrates with thiolate self-assembled monolayers (SAMs) on the properties of nanoporous thin films derived from polystyrene-*block*-poly(ethylene oxide) having a photocleavable *o*-nitrobenzyl ester junction (PS-*hν*-PEO). Two PS-*hν*-PEO having similar PEO volume fractions (≈0.2) but different molecular weights (10 and 23 kg/mol) were used to prepare films (30−100 nm thick) spin-cast on gold substrates unmodified and modified with cysteamine, thioctic acid, and 6-hydroxy-1-hexanethiol SAMs. Solvent vapor annealing followed by PEO removal led to the formation of nanopores with average diameters of 12 and 19 nm from the smaller and larger PS-*hν*-PEO, respectively. Cyclic voltammograms of 1,1′-ferrocenedimethanol showed that nanoporous films on cysteamine SAMs afforded nanopores reaching the underlying substrates at higher density than those on the other substrates. This result was attributed to balanced affinity of the cysteamine SAM surface with PS and PEO, which enhanced the vertical orientation of PEO microdomains. The generation of carboxyl groups associated with the photocleavage reaction was revealed by pH-dependent changes in the voltammogram of $Fe(CN)_6^{3-}$ that reflected electrostatic effects regulated by the protonation state of the carboxyl groups. The SAMs underneath the nanoporous films could be replaced by treatment with a thiol solution, as verified by voltammograms of L-ascorbic acid. These results suggest that thiolate SAM modification provides a simple means to control the interfacial orientation of PEO microdomains in thin PS-*hν*-PEO films.

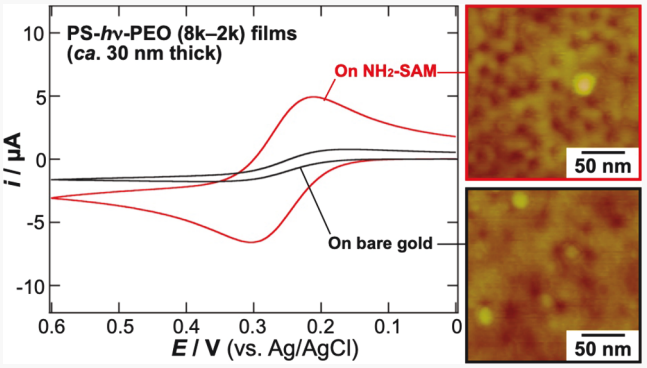

INTRODUCTION

Microphase separation of block copolymers provides a unique means to fabricate periodic nanostructures having predictable morphologies and uniform dimensions.[1] The morphologies and dimensions of the nanostructures, microdomains, can be rationally controlled by adjusting the incompatibility and lengths of the constituent polymer blocks. In particular, substrate-supported nanoporous thin films derived from block copolymers have been explored for various applications, including masks for nanolithography,[2,3] templates for nanomaterial fabrication,[4−6] membranes for chemical separations,[7−9] and platforms for electrochemical sensing.[6,8,10] These applications utilize nanopores that are formed upon the selective removal of cylindrical (or gyroid) microdomains.[11] Such nanoporous films are often prepared by degrading the sacrificial blocks of block copolymers such as polystyrene-*block*-poly(methyl methacrylate) (PS-*b*-PMMA),[12] polystyrene-*block*-polylactide (PS-*b*-PLA),[13] polystyrene-*block*-poly(ethylene oxide) (PS-*b*-PEO),[14] and polystyrene-*block*-poly(dimethylsiloxane) (PS-*b*-PDMS).[15] However, degradation of these blocks requires fairly harsh conditions such as UV-C irradiation (for PMMA),[12] or treatment in concentrated base (for PLA)[13] or acid (for PEO and PDMS),[14,15] which limits the selection of underlying supports to chemically robust materials. This limitation can be mitigated by use of block copolymers incorporating cleavable junctions that permit the removal of minor blocks under mild conditions using a weak acid,[16] a reducing agent,[17] and UV-A.[18−20] Among them, PS-*b*-PEO with a photocleavable *o*-nitrobenzyl ester (ONB) junction, PS-*hν*-PEO, has been studied extensively for the fabrication of nanoporous thin films.[18,20,21] The surfaces of the resulting nanoporous films can be further tailored *via* postfunctionalization.[21−24] However, PS-*hν*-PEO-derived nanoporous films have been explored only for photopatterning[21,22] and silica nanodot fabrication,[20] both of which do not

Received: May 27, 2020
Revised: July 15, 2020
Published: July 18, 2020

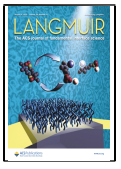

https://dx.doi.org/10.1021/acs.langmuir.0c01572
Langmuir 2020, 36, 9259−9268

require nanopores that expose the underlying substrates in contrast to other applications such as electrochemical sensing.[6,8,10]

Many of the applications being considered seek to take advantage of nanopores that are formed from cylindrical microdomains that vertically penetrate through a thin block copolymer film. A number of approaches have been established to enhance the vertical orientation of cylindrical microdomains in substrate-supported thin films,[25] including electric field application during thermal annealing[12] and directional solvent vapor evaporation (solvent vapor annealing, SVA).[26,27] In addition, substrate surface properties need be adjusted to control microdomain orientation at the film−substrate interface and also to obtain uniform thin films without dewetting.[28] A neutral surface, which has similar affinities to constituent block copolymer blocks, is often employed to prepare thin films with vertically oriented microdomains.[29] Such surfaces have been obtained by covalently grafting them with random copolymer brushes of appropriate monomer fractions[30] or organosilane monolayers.[31] However, these surface grafting methods afford relatively thick insulating layers that remain upon the removal of cylindrical microdomains and thus are not suitable to prepare nanoporous thin films for electrochemical applications. Vertically oriented cylindrical microdomains were obtained on substrates coated with indium tin oxide or gold without surface grafting by using the application of electric fields[32,33] or owing to nanoscale surface roughness.[34,35] However, the former needs a sophisticated setup to apply a high voltage across a thin film at high temperature[32,33] and the latter requires optimization of the annealing conditions to attain the metastable structure.[35] For these reasons, routine access to vertically aligned microdomains on electrically conductive substrates remains an outstanding challenge.

In this study, we prepared nanoporous thin films (Figure 1) using PS-*hν*-PEO deposited on gold substrates that were modified with thiolate self-assembled monolayers (SAMs). Thiolate SAMs have not been widely examined for the purpose of obtaining neutral surfaces for controlling block copolymer microdomains[36,37] because of their limited thermal stability.[38,39] Many previous studies were carried out using block copolymers that require thermal annealing at high temperature (often >160 °C) for their microphase separation. In contrast, PS-*b*-PEO does not require thermal annealing to achieve microphase separation, and the orientation of its PEO microdomains can be improved using SVA at room temperature.[40,41] Indeed, micropatterned surfaces with long alkanethiol SAMs were used to manipulate the distribution of PS-*b*-PEO droplets based on the dewetting of the solvent-swollen polymer.[42,43] Herein, PS-*hν*-PEO was used to fabricate nanoporous thin films under relatively mild conditions involving SVA and UV-A irradiation (Figure 1a−c), which would cause negligible damage to underlying substrates.[18,20,21] Nanoporous thin films were prepared on gold substrates modified with cysteamine, thioctic acid, and 6-hydroxy-1-hexanethiol SAMs (Figure 1d), denoted as NH_2-, OH-, and COOH-SAMs, respectively, in addition to bare gold substrates. The polar terminal groups of these SAMs would reduce the affinity of PS to inhibit the formation of an insulating PS layer on the substrate surfaces. More importantly, their alkyl chains are short enough to allow electrode reactions,[44−49] and thus, the properties of nanoporous films can be assessed using electrochemical methods. Atomic force microscopy (AFM), Fourier-transform infrared external reflection spectroscopy (FTIR-ERS), and cyclic voltammetry (CV) were used to characterize polymer thin films on these substrates. In particular, CV provides a simple means to assess the permeability of the electrode-supported nanoporous film and the electrochemical activity of the underlying substrate, which provide insight into microdomain orientation at the film−substrate interface.[35,50] This study reveals the applicability of PS-*hν*-PEO-derived nanoporous films as electrochemical sensing layers that have the potential to be used to improve detection sensitivity and selectivity, as shown with other polymer-based or inorganic nanoporous films.[6,10,51−53]

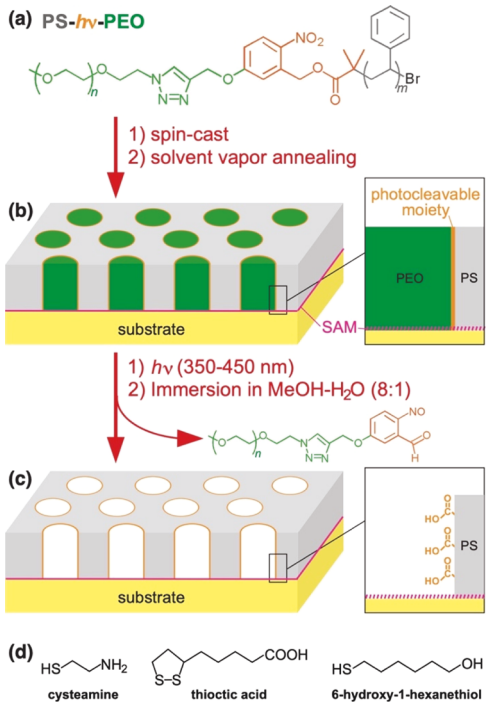

Figure 1. (a−c) Molecular structure of PS-*hν*-PEO used in this study and procedure for the preparation of a nanoporous thin film: (b) fabrication of a thin PS-*hν*-PEO film comprising PEO microdomains using spin-casting onto a gold substrate modified with a thiolate SAM, followed by SVA under a benzene/water atmosphere to enhance microphase separation and vertical microdomain orientation; (c) removal of the PEO microdomains using UV-A irradiation at 350−450 nm, followed by immersion in methanol−water (8:1). (d) Molecular structures of cysteamine, thioctic acid, and 6-hydroxy-1-hexanethiol, which were used to obtain NH_2-, COOH-, and OH-SAMs, respectively.

EXPERIMENTAL SECTION

Chemicals and Materials. Two PS-*hν*-PEO having similar PEO volume fractions but different molecular weights [PS-*hν*-PEO (8k−2k) and PS-*hν*-PEO (18k−5k); Table 1] were synthesized by atom transfer radical polymerization (ATRP)[19] according to a synthetic procedure described in Scheme 1. Detailed synthesis of PS-*hν*-PS including its characterization can be found in the Supporting Information. Cysteamine (Aldrich and TCI America), thioctic acid (Acros), 6-hydroxy-1-hexanethiol (Aldrich), 1,1′-ferrocenedimethanol ($Fc(CH_2OH)_2$, Aldrich), potassium ferricyanide ($K_3Fe(CN)_6$, Acros), L-ascorbic acid (L-AA, Acros), *o*-phosphoric acid (Fisher), and diiodomethane (Alfa Aesar) were used as received. All other chemicals were of reagent grade and used as received. Gold-coated silicon wafers, which were prepared by sputtering 10 nm of Ti followed by 200 nm of Au onto Si (100) wafers, were purchased from LGA Thin Films (Foster City, CA). All aqueous solutions were

https://dx.doi.org/10.1021/acs.langmuir.0c01572
Langmuir 2020, 36, 9259−9268

Table 1. PS-*hν*-PEO and the Properties of Its Nanoporous Thin Films

polymer	M_{PS}[a] (kg/mol)	M_{PEO} (kg/mol)	f_{PEO}[b]	PDI[c]	pore diameter (nm)[d,e]	pore density (pores/μm^2)[d]
PS-*hν*-PEO (8k−2k)	7.8	2.0	0.19	1.15	12 ± 1	1300
PS-*hν*-PEO (18k−5k)	18.0	5.0	0.20	1.20	19 ± 2	1000

[a]Determined from ^{1}H NMR spectra. [b]Calculated with the density of PS (1.04 g/cm^3) and PEO (1.22 g/cm^3). [c]Determined using gel permeation chromatography. [d]Determined from the AFM images of PS-*hν*-PEO-derived nanoporous films on NH_2-SAMs. [e]Average and standard deviation obtained from ≥29 pores.

Scheme 1. Synthetic Route for PS-*hν*-PEO *via* ATRP of Styrene from PEO-ONB-Br

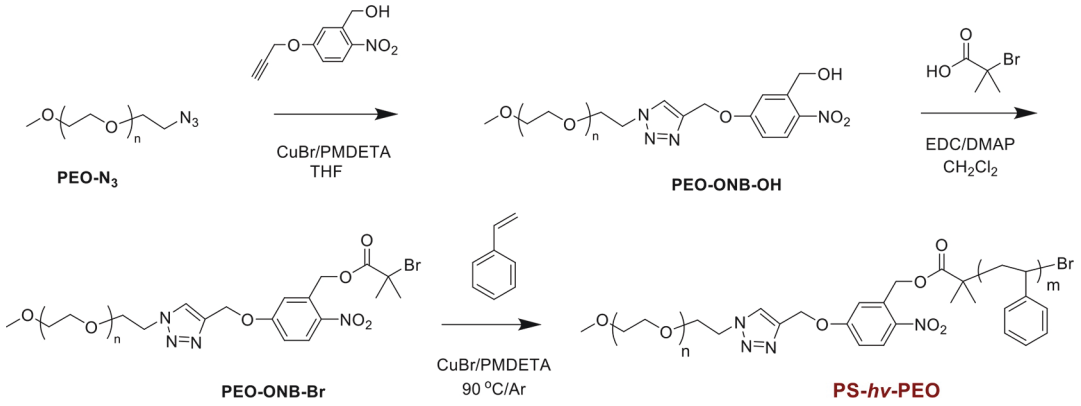

prepared with water having a resistivity of 18 MΩ (Barnstead Nanopure systems).

Thin-Film Preparation (Figure 1a−c). Gold-coated silicon substrates (*ca.* 1.2 × 1.2 cm^2) were cleaned using a Novascan PSD-UVT UV−ozone system for 20 min. SAM modification was carried out by immersing the cleaned substrates in a 5 mM ethanol solution of cysteamine, thioctic acid, or 6-mercapto-1-hexanol overnight.[39] The substrates were thoroughly washed with ethanol and dried under an Ar stream. Thin PS-*hν*-PEO films were prepared on these substrates by spin-coating (2000 rpm, 30 s) from its toluene solution (0.5−2 wt %) and then annealed in a benzene/water atmosphere (relative humidity: 75−85%) in a desiccator for 3 h at room temperature (21−25 °C).[41] Of note, an increase in microdomain diameter was observed after SVA for ≥4 h (data not shown) owing to the swelling of PEO microdomains by water.[40,41] Nanoporous thin films were obtained by the selective removal of PEO by UV irradiation using a Newport UV photography system with a near-UV source (λ = 350−450 nm, 76 mW/cm^2) for 3 h and subsequent immersion in methanol−water (8:1).[18] UV light at 350−450 nm was used rather than that at 300 nm[19,21] to prevent side reactions postulated to occur from the UV−vis absorption spectra of PS-*hν*-PEO solution upon UV irradiation at 300 and 365 nm (Figure S8). The UV irradiation and subsequent immersion were conducted twice to maximize the removal of the PEO microdomains.

Thin-Film Characterization. Ellipsometric film thickness was measured using a J. A. Woollam alpha-SE spectroscopic ellipsometer. Film thicknesses given in this paper were the ellipsometric thickness of an as-cast film obtained using the Cauchy model. The refractive index (n) values of the as-cast PS-*hν*-PEO films (*ca.* 30 nm thick) were 1.555 ± 0.010 (for 8k−2k) and 1.551 ± 0.005 (for 18k−5k) (95% confidence interval obtained from 10 to 30 different films), respectively, which are close to that (1.562) estimated from f_{PEO} (=0.2) and the n values of PS (1.589) and PEO (1.454). Interestingly, the PEO removal process negligibly changed the n values of PS-*hν*-PEO (8k−2k) films (1.551 ± 0.012) but significantly decreased those of PS-*hν*-PEO (18k−5k) films (1.515 ± 0.007). The concomitant decrease in ellipsometric thickness was more significant for PS-*hν*-PEO (8k−2k) films (*ca.* 15%) than PS-*hν*-PEO (18k−5k) films (*ca.* 10%). The underlying substrates did not give significant influences on the changes in ellipsometry data. AFM images were obtained by tapping-mode imaging in air, using a Digital Instruments Multimode AFM with Nanoscope IIIa electronics. Tapping-mode AFM probes were purchased from Asylum. FTIR-ERS measurements of thin films were carried out using a Nicolet iS50 FTIR spectrophotometer equipped with a Harrick Seagull reflection accessory (Pleasantville, NY) purged with N_2 and a DTGS detector. A cleaned gold-coated silicon substrate was used to measure background spectra. All spectra were the sum of 256 scans obtained with 4 cm^{-1} resolution at an 84° angle of incidence with respect to the gold substrate. Sessile drop contact angles were measured according to a reported procedure.[54]

Electrochemical Measurements. CV measurements were performed in a three-electrode cell containing a Ag/AgCl (1 M KCl) reference electrode and a Pt counter electrode using a CH Instruments model 618B electrochemical analyzer. A gold substrate with or without PS-*hν*-PEO-derived nanoporous film was immobilized at the bottom of the cell to serve as the working electrode.[50] The area of a film-coated electrode in contact with the solution was 0.33 cm^2, which was defined by an O-ring used for the cell (0.65 cm in diameter). Of note, the electroactive area of an underlying electrode could not be determined from the amount of charge associated with the reduction of the gold surface oxide[55] or the reductive desorption of thiols,[56,57] probably because the solution used for these measurements leached to the film−substrate interface upon the application of a relatively large anodic or cathodic potential. The pH of a solution containing 0.1 M KCl and 10 mM phosphate was adjusted by adding a KOH solution using a Denver Instrument UB-10 pH/mV meter with a Fisher Accumet pH glass electrode. The replacement of underlying SAMs was explored by treating film-coated electrodes with an aqueous solution of 1 mM 6-hydroxy-1-hexanethiol or with an ethanol solution of 5 mM cysteamine for ≥3 h,[45] followed by washing the electrodes with water prior to CV measurements.

RESULTS AND DISCUSSION

Synthesis of PS-*hν*-PEO and Preparation of Nanoporous Thin Films. A one-pot synthetic strategy of PS-*hν*-PEO was reported by Schumers *et al.*,[19] in which ATRP of styrene and copper-catalyzed alkyne−azide cycloaddition (CuAAC) was conducted simultaneously. However, the strategy generated homopolymers which needed to be removed from the final product. In this study, PS-*hν*-PEO was instead synthesized by ATRP of styrene from a PEO macroinitiator, PEO-ONB-Br, which afforded a product without further purification. PEO-ONB-Br was prepared in

https://dx.doi.org/10.1021/acs.langmuir.0c01572
Langmuir 2020, 36, 9259−9268

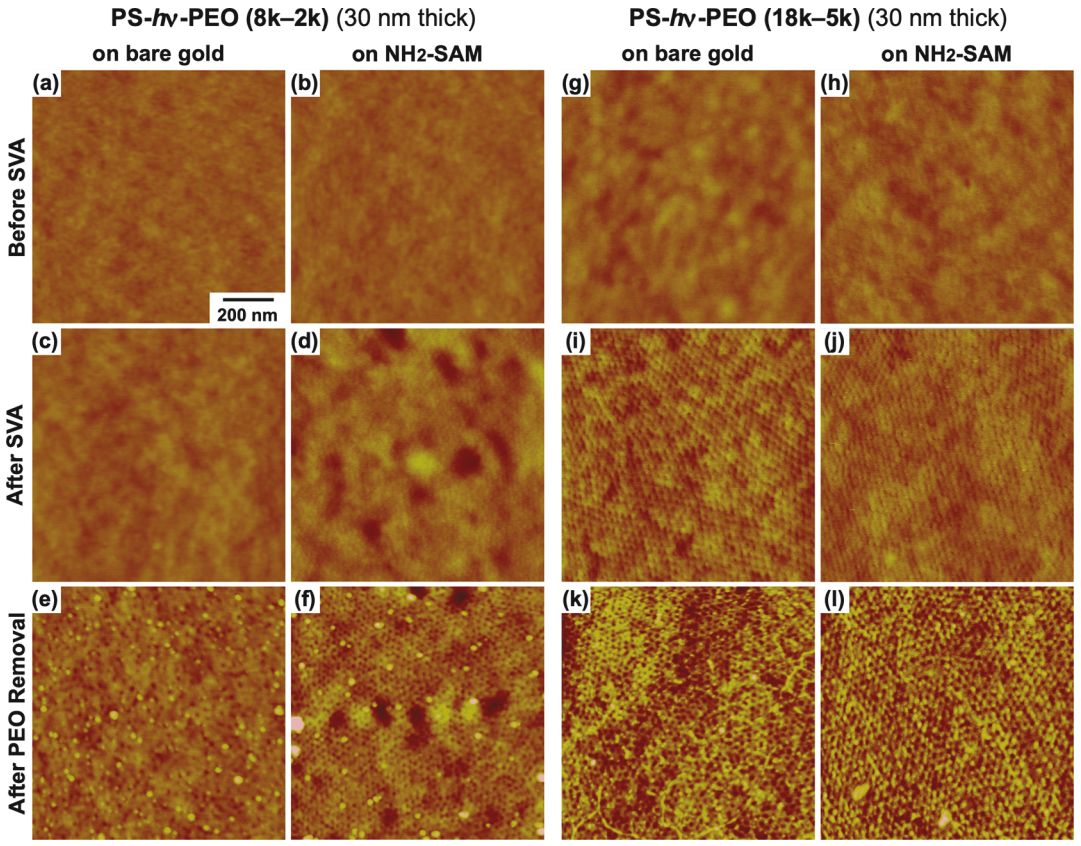

Figure 2. AFM height images ($1 \times 1\ \mu m^2$; $\Delta z = 20$ nm) of thin films (30 nm thick) of (a–f) PS-*hν*-PEO (8k–2k) and (g–l) PS-*hν*-PEO (18k–5k) on bare gold (left) and cysteamine SAMs (right) before and after SVA using benzene–water vapor for 3 h and after removing PEO *via* duplicated UV irradiation and subsequent soaking in methanol–water (8:1). Phase images simultaneously obtained with these height images are shown in Figure S9. Of note, nanoscale particles on the PS-*hν*-PEO (8k–2k) films (e,f) could be removed by immersing in water (data not shown). These particles did not have significant influence on FTIR-ERS spectra.

two steps as shown in Scheme 1. First, PEO-ONB-OH was made by CuAAC reaction of poly(ethylene glycol) methyl ether azide (PEO-N_3) and 5-propargyloxy-2-nitrobenzyl alcohol. Then, EDC coupling of PEO-ONB-OH and 2-bromoisobutyric acid produced PEO-ONB-Br. ATRP of styrene at 90 °C from two PEO-ONB-Br macroinitiators that have molecular weight of 2k and 5k afforded PS-*hν*-PEO (8k–2k) and PS-*hν*-PEO (18k–5k) (Table 1).

The synthesized PS-*hν*-PEO was spin-cast from its toluene solution on gold substrates unmodified and modified with SAMs to obtain its thin films. The thin films were subsequently annealed in a benzene/water atmosphere to enhance the formation and vertical orientation of PEO microdomains (Figure 1b).[41] The resulting PEO microdomains were selectively removed (Figure 1b) by UV-A irradiation, which involves the photoisomerization of the *o*-nitrobenzyl ester into *o*-nitrosobezaldehyde,[58] followed by their dissolution in methanol–water (8:1).[18] As shown in Figure 1c, the photocleavage reaction generates carboxyl groups on the nanopore surface.

Effects of SVA and PEO Removal on the Surface Morphologies of PS-*hν*-PEO Films. First, the surface morphologies of PS-*hν*-PEO films were studied at each of the sample preparation steps (Figure 1a–c) using tapping-mode AFM. Figures 2a–f and S9a–f show AFM height and phase images, respectively, of PS-*hν*-PEO (8–2k) films (30 nm thick) formed on bare gold substrates and NH_2-SAMs. The PS-*hν*-PEO (8k–2k) film did not exhibit clear surface features prior to SVA (Figures 2a,b and S9a,b). This result suggests that this polymer was too short for microphase separation[59] as indicated by the small χN (≈7.7) estimated from the Flory–Huggins interaction parameter of PS-*b*-PEO ($\chi \approx 0.0645$ at 25 °C)[60] and its repeating units ($N \approx 119$). Upon SVA under a benzene/water atmosphere, a thin film on a NH_2-SAM showed sub-μm-scale shallow depressions (<5 nm deep and 50–200 nm in diameter) in the height image (Figure 2d), and more interestingly, small periodic features (10–20 nm) in the phase images (Figure S9d). The observation of the small features indicates the SVA-induced formation of microdomains based on the preferential incorporation of water into PEO in the benzene-swollen film. UV-A irradiation (λ = 350–450 nm) and subsequent immersion in methanol–water (8:1) led to the formation of nanoscale pores in these films (Figures 2e,f and S9e,f) after the removal of the PEO microdomains. Interestingly, the thin film on NH_2-SAM comprised nanopores (*ca.* 12 nm in diameter) at a higher density (1300 pores/μm^2; Table 1 and Figure 2f) than that on bare gold (*ca.* 15 nm in pore diameter, 500 pores/μm^2; Figure 2e). Such nanopores were not observed in 30 nm films formed on OH– and COOH-SAMs (Figure S10c,d). These observations imply that the surface of NH_2-SAM had balanced affinities to solvent-swollen PS and PEO, facilitating the vertical orientation of cylindrical PEO microdomains. NH_2-SAM does not have a high affinity to PEO, which we attribute to insufficient hydrogen bonding with the ether moieties of PEO. In contrast, the other surfaces cannot efficiently afford vertically oriented

https://dx.doi.org/10.1021/acs.langmuir.0c01572
Langmuir 2020, 36, 9259–9268

PEO microdomains probably because of the significantly higher affinity to one of the two polymer blocks: the bare gold surface has a higher affinity to PS, whereas the OH- and COOH-SAMs have a very high affinity to PEO through hydrogen bonds formed between their terminal donor groups and PEO ethers.[42,43] There was no clear correlation between the PEO microdomain orientation and the surface free energies of these substrates determined from contact angle data (Table S1),[61,62] supporting the significant contributions of hydrogen bonding interactions to these observations. The AFM images of 50 nm films on these substrates (Figure S10a,b) are similar to those of 30 nm films but also showed horizontally oriented nanotrenches in Figure S10b, suggesting the deterioration of the vertical microdomain orientation in the thicker film.

In contrast to thin films of PS-*hν*-PEO (8k−2k), disordered microdomains were observed from the as-cast PS-*hν*-PEO (18k−5k) films on bare gold and NH_2-SAM (Figures 2g,h and S9g,h), suggesting that the polymer is long enough to give microdomains in the as-cast films ($N \approx 287$; $\chi N \approx 18.5$). Vertically oriented microdomains and nanopores with an average diameter of 19 nm (Table 1) were observed after SVA (Figures 2i,j and S9i,j) and the subsequent removal of the PEO microdomains (Figures 2k,l and S9k,l). Interestingly, there was no clear difference between the AFM images of PS-*hν*-PEO (18k−5k) films on these different substrates, probably because the surface morphologies were determined by directional solvent evaporation during the SVA process.[40,41] In spite of the similarity of the AFM images, the underlying substrates seemed to give significant influences on microdomain structure at the film−substrate interface also for PS-*hν*-PEO (18k−5k), as suggested by electrochemical data shown in the later section.

FTIR-ERS Spectra of PS-*hν*-PEO Films before and after PEO Removal. FTIR-ERS was used to verify the removal of PEO microdomains promoted by UV-A irradiation and subsequent immersion in methanol−water (8:1). Figure 3 shows FTIR-ERS spectra of PS-*hν*-PEO (8k−2k) films (30 nm thick) on (a) bare gold and (b) NH_2-SAM before and after the PEO removal process. The FTIR-ERS spectra of thin PS-*hν*-PEO films were almost identical before and after SVA (data not shown). The PEO removal process led to the reduction of absorption bands associated with PEO, including aliphatic C−H stretching bands from PS and PEO at 2800−3000 cm^{-1} and C−C/C−O stretching bands from PEO at 1100−1200 cm^{-1}.[21,63] The latter band did not completely disappear even after repeated UV-A irradiation and methanol−water soaking, suggesting the presence of residual PEO. Similar changes in FTIR-ERS spectra were observed for PS-*hν*-PEO (8k−2k) films with different thicknesses (Figure S11a,b) or on COOH- and OH-SAMs (Figure S11c,d), and for PS-*hν*-PEO (18k−5k) films (Figure S11e,f). The efficiency of PEO removal, which was estimated from the absorbance ratio of a C−H stretching band of PS at 3026 cm^{-1} and a C−O/C−C stretching band of PEO at 1112 cm^{-1}, was 60−80%. Unfortunately, the efficiency could not be quantitatively compared between different polymers or among different substrates owing to a large error associated with difficulty in reliable baseline subtraction. The presence of residual PEO on any of the underlying substrates however implies imperfect microphase separation and/or microdomain orientation. Overall, the FTIR-ERS data supported the removal of PEO microdomains by the extraction of photocleaved PEO, but also revealed the presence of residual PEO in the nanoporous films.

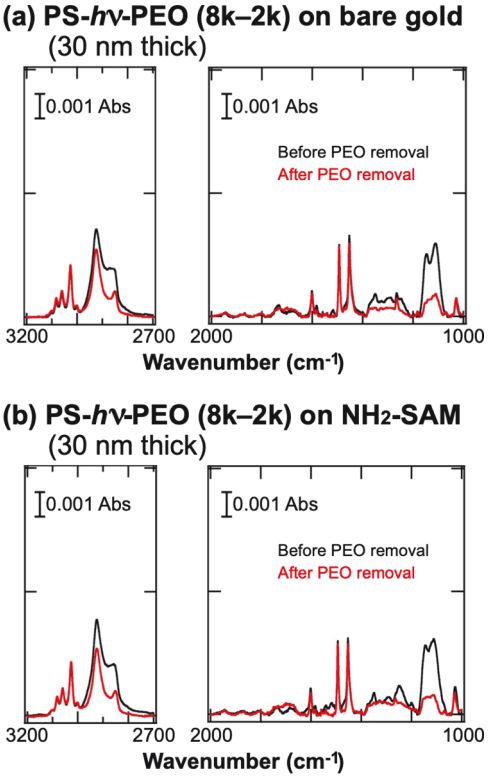

Figure 3. FTIR-ERS spectra of PS-*hν*-PEO (8k−2k) films (30 nm thick) before (black) and after (red) PEO removal (a) on bare gold and (b) on NH_2-SAM.

Cyclic Voltammograms of 1,1′-Ferrocenedimethanol for Evaluation of the Permeability of PS-*hν*-PEO-Derived Nanoporous Films on Different Substrates. The AFM and FTIR-ERS results clarified the formation and selective removal of PEO microdomains in PS-*hν*-PEO thin films. However, these methods cannot provide information on the film−substrate interfaces that control the solute permeability of the nanoporous films and the electroactivity of the underlying electrodes. Here, CV was used to investigate the effects of the underlying substrates on film permeability and electrode electroactivity,[50] which would help provide insights into the orientation of the microdomains on the different substrates. The ferrocene-based redox probe, $Fc(CH_2OH)_2$, is uncharged, and thus, it can be used to assess nanopore permeability with negligible influence of electrostatic interactions.[50,64]

Figure 4 shows cyclic voltammograms of $Fc(CH_2OH)_2$ (a) for nanoporous films (30 nm thick) formed from PS-*hν*-PEO (8k−2k) on bare gold and the three SAMs and (b) for nanoporous films (30 nm thick) formed from PS-*hν*-PEO (18k−5k) on bare gold and NH_2-SAM. The nanoporous films on the NH_2-SAMs exhibited peak-shaped voltammograms (Figure 4a,b; depicted in red). This behavior contrasts with those seen from the other three substrates, which gave more sigmoidal voltammograms with smaller faradaic currents. The observation of the peak-shaped voltammograms typically indicates the presence of highly dense active nanopores that led to the overlapping of diffusion layers developed from individual electroactive underlying electrodes.[10,65] Alternatively, the faradaic currents of the peak-shaped voltammograms were smaller than those observed at a planar gold substrate of the identical geometric area (Figure 4a; depicted in purple),

https://dx.doi.org/10.1021/acs.langmuir.0c01572
Langmuir 2020, 36, 9259−9268

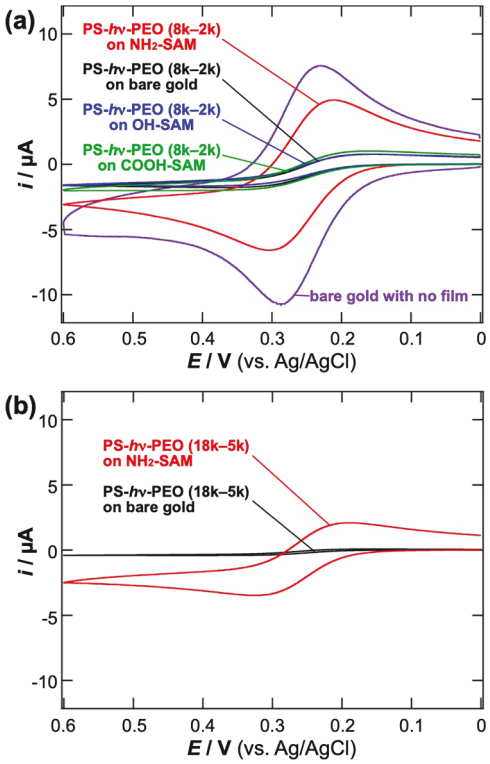

Figure 4. Cyclic voltammograms (ν = 0.02 V/s) of 0.3 mM $Fc(CH_2OH)_2$ measured in 0.1 M KCl + 10 mM phosphate (pH 7.0) at room temperature. (a) Cyclic voltammograms for nanoporous films (30 nm thick) formed from PS-*hν*-PEO (8k−2k) on bare gold (black), NH_2-SAM (red), OH-SAM (blue), and COOH-SAM (green), in addition to one obtained at a bare gold substrate with no polymer film (purple). (b) Cyclic voltammograms for nanoporous films (30 nm thick) formed from PS-*hν*-PEO (18k−5k) on bare gold (black) and NH_2-SAM (red).

reflecting the partial blocking of the electrode surface by a nanoporous insulating layer.[66,67] The higher permeability and electroactivity obtained from nanoporous films on NH_2-SAM reflect the vertical orientation of PEO microdomains enhanced at the interface, as suggested by the AFM data (see above).

The thicker nanoporous films on NH_2-SAM exhibited sigmoidal voltammograms with smaller faradaic currents (Figure S12), suggesting a decrease in the density of active nanopores. The lower density of active nanopores, together with the observation of horizontal nanotrenches using AFM (Figure S10b), could reflect the deterioration of microdomain orientation during the longer solvent evaporation from the thicker films: presumably the longer drying time led to a gradual change in the solvent compositions of the PS and PEO microdomains, which altered their affinities to the NH_2-SAM surface and thus gave disordered microdomain morphologies.[68]

Cyclic Voltammograms of $Fe(CN)_6^{3-}$ at Different pH Conditions for Investigation of Functional Groups Generated in PS-*hν*-PEO-Derived Nanoporous Films. The photocleavage reaction of the *o*-nitrobenzyl ester junction of PS-*hν*-PEO is anticipated to yield carboxyl groups on the exposed cylindrical surfaces of the nanopores, as illustrated in Figure 1c. Unfortunately, the FTIR-ERS spectra did not show clear changes in C═O stretching vibration bands following PEO removal, though a broader band observed at 1700−1750 cm^{-1} for PS-*hν*-PEO (8k−2k) (Figures 3 and S11a−d) may be associated with the carboxyl groups. The presence of the carboxyl groups in the nanoporous films was examined by CV measurements with anionic $Fe(CN)_6^{3-}$ at different pH.[50,64]

Figure 5 shows cyclic voltammograms of $Fe(CN)_6^{3-}$ for a nanoporous film (30 nm thick) derived from PS-*hν*-PEO (8k−2k) on NH_2-SAM at pH 2.3−7. The faradaic current of $Fe(CN)_6^{3-}$ increased with decreasing pH from 7 to 2.3 with more significant changes from pH 6 to 3. The pH-dependent change was reversible, as shown by current recovery observed when the pH was changed from 2.3 to 7. The pH-dependence of the CV data of $Fe(CN)_6^{3-}$ was not a consequence of a change in nanopore structure, as indicated by the similar CVs acquired from the uncharged $Fe(CH_2OH)_2$ across the same pH range (Figure S13). More importantly, similar pH-dependent voltammograms of $Fe(CN)_6^{3-}$ were observed for nanoporous films (30 nm thick) formed from PS-*hν*-PEO (8k−2k) on bare gold and nanoporous films (30 nm thick) formed from PS-*hν*-PEO (18k−5k) on NH_2-SAM, but not at a bare gold electrode without nanoporous film (Figure S14). These observations were consistent to the presence of carboxyl groups in PS-*hν*-PEO-derived nanoporous films.[50,64] The decrease in pH led to the protonation of the $-COO^-$ groups (pK_a = 4−5), which reduced electrostatic repulsion to allow the permeation of $Fe(CN)_6^{3-}$.

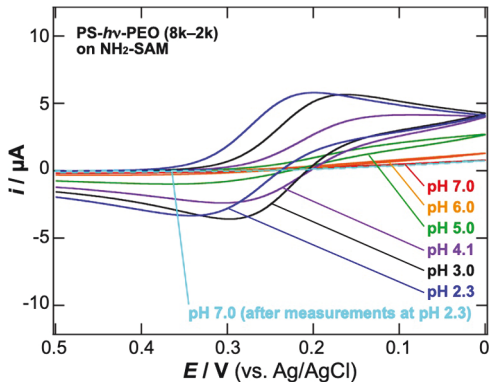

Figure 5. Cyclic voltammograms (ν = 0.02 V/s) of 0.3 mM $K_3Fe(CN)_6$ at different pH (pH 2.3−7) that were measured for nanoporous films (30 nm thick) formed from PS-*hν*-PEO (8k−2k) on NH_2-SAM. Measured in 0.1 M KCl + 10 mM phosphate at room temperature.

Interestingly, the faradaic reaction of $Fe(CN)_6^{3-}$ was almost entirely blocked at pH 7 (Figures 5 and S14a,b). The nanopore radii (6 and 9.5 nm) were significantly larger than the Debye length in 0.1 M KCl (*ca.* 1 nm). Therefore, these nanoporous films were anticipated to exhibit peak-shaped voltammograms with smaller faradaic currents at higher pH, as observed for PS-*b*-PMMA-derived nanoporous films with similar nanopore diameters.[50] The highly efficient electrostatic blocking at pH 7 implied the presence of a carboxyl-containing polymer residue coated onto the underlying substrate. This residue was permeable for uncharged species such as $Fe(CH_2OH)_2$ but could electrostatically control the permeability of anionic species. The presence of the polymer residue might be associated with incomplete microphase separation between PS and PEO at the interfacial region, as realized in the applications of block copolymers as lithographic masks and polyelectrolytes.[69,70]

https://dx.doi.org/10.1021/acs.langmuir.0c01572
Langmuir 2020, 36, 9259−9268

CV Measurements of L-Ascorbic Acid for Assessment of the Replacement of Underlying SAMs. The observation of faradaic currents in the CV measurements (Figures 4 and 5) indicates that redox-active species can diffuse through the nanoporous films and react at the underlying SAM-modified gold substrates. In addition, the CV data of $Fe(CN)_6^{3-}$ implies the presence of a polymer residue that can electrostatically manipulate the diffusion and/or electrode reaction of the anionic redox-active species. However, it is unclear whether the polymer residue controlled the electron transfer process of $Fe(CN)_6^{3-}$. The roles of the underlying SAMs in electrode reactions were investigated by measuring the CV data of L-ascorbic acid (L-AA) after treating the polymer-coated substrates with thiol solutions.[45] The rationale for this measurement is that cyclic voltammograms of L-AA were found to be sensitive to the types of SAMs on the electrodes.[46]

Figure 6a shows cyclic voltammograms of L-AA for a nanoporous film (30 nm thick) formed from PS-*hν*-PEO (18k−5k) on NH_2-SAM before and after treatment with a 6-hydroxy-1-hexanethiol solution (red and blue, respectively) and after treatment with a cysteamine solution (green). These voltammograms did not show the anodic peak of L-AA in contrast to a cysteamine-modified gold disk electrode,[46] probably because the anionic polymer residue at pH 7 electrostatically reduced the diffusion of anionic L-AA, as with $Fe(CN)_6^{3-}$ (Figure 5). Importantly, the anodic current of L-AA decreased after treatment with the 6-hydroxy-1-hexanethiol and then increased after subsequent treatment with cysteamine solutions. These results indicate that the initial NH_2-SAM could be successfully replaced with an OH-SAM, and then the OH-SAM could be replaced with a NH_2-SAM. It should be noted that these same treatments did not affect the cyclic voltammograms of $Fc(CH_2OH)_2$ (Figure 6b), indicating that the nanoporous film was stable in the aqueous and ethanolic solutions. Very similar results were obtained for a nanoporous film (30 nm thick) formed from PS-*hν*-PEO (8k−2k) (Figure S15). Indeed, negligible changes in the AFM images of PS-*hν*-PEO-derived nanoporous films were observed after immersion in the aqueous and ethanolic solutions or in 2-propanol (data not shown), in contrast to a paper reporting the structural instability of similar films formed on oxide-coated silicon substrates.[71] The successful replacement of the underlying SAMs indicates that the SAMs were exposed and accessible after the UV-initiated PEO removal process. Of note, we did not explore or confirm the complete replacement of the SAMs, on account of the fact that the CV measurements with L-AA aimed to verify the involvement of the underlying SAMs in electrode reactions. The postfunctionalization of the underlying substrates by SAM replacement as well as the nanoporous polymer films by pH change can be used to control electrode reactions and solute diffusion for the purpose of designing electrochemical sensors with PS-*hν*-PEO, as demonstrated with other block copolymer-derived nanoporous films[10] and other types of materials.[51−53]

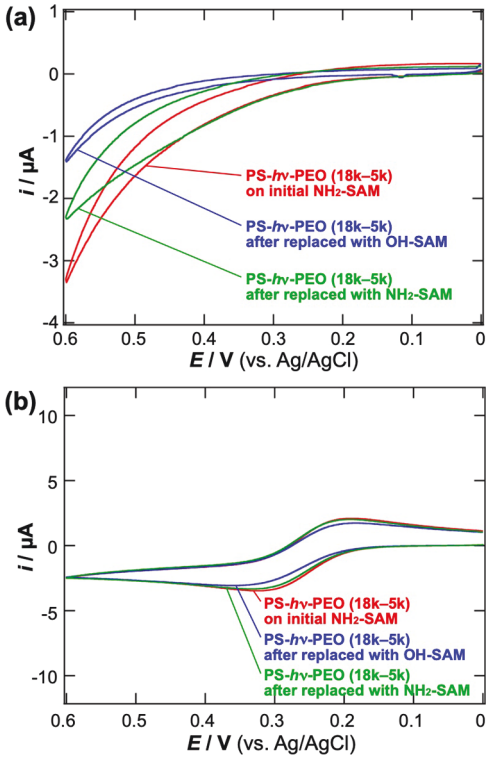

Figure 6. Cyclic voltammograms (0.02 V/s) of (a) 1.3 mM L-AA and (b) 0.3 mM $Fc(CH_2OH)_2$ for a nanoporous film (30 nm thick) formed from PS-*hν*-PEO (18k−5k) on NH_2-SAM (red), after treatment with 1 mM 6-hydroxy-1-hexanethiol in water for 3 h (blue) and subsequent treatment with 5 mM cysteamine in ethanol for 3 h (green). Measured in 0.1 M KCl + 10 mM phosphate (pH 7.0) at room temperature.

CONCLUSIONS

This study demonstrates that the NH_2-SAM modification of gold substrates provides a simple means to prepare PS-*hν*-PEO thin films comprising vertically oriented PEO microdomains at the film−substrate interface using SVA. The PEO microdomains can be selectively removed following photocleavage to afford nanoporous thin films, as characterized using AFM, FTIR-ERS, and CV. A series of CV measurements revealed the effects of the underlying SAM-coated substrates on the solute permeability of the nanoporous thin films, the presence of carboxyl groups after the photocleavage reaction, the high stability of the nanoporous films in water and ethanol, and the capability to postfunctionalize the underlying substrates. In addition, these measurements indicated challenges in material design, including the limited thickness range for fabrication of highly permeable nanoporous films and the presence of a polymer residue that could manipulate solute accessibility to the underlying substrates. The integration of the photopatterning capability[21,22] with the postfunctionalization of the underlying substrates and nanoporous films will provide a unique means to design novel electrochemical microsensor arrays using PS-*hν*-PEO.

ASSOCIATED CONTENT

Supporting Information

The Supporting Information is available free of charge at https://pubs.acs.org/doi/10.1021/acs.langmuir.0c01572.

Synthetic procedure for PS-*hν*-PEO and its NMR and GPC data, UV−vis spectra of PS-*hν*-PEO solutions at different periods of UV irradiation, AFM phase images, AFM height images of PS-*hν*-PEO (8k−2k) films with different thicknesses on different substrates, FTIR-ERS spectra of PS-*hν*-PEO (8k−2k) films with different thicknesses on different substrates and PS-*hν*-PEO (18k−5k) films with *ca.* 30 nm thick on bare gold and

https://dx.doi.org/10.1021/acs.langmuir.0c01572
Langmuir 2020, 36, 9259−9268

NH_2-SAM, cyclic voltammograms of $Fc(CH_2OH)_2$ for PS-*hν*-PEO (8k−2k)-derived nanoporous films on NH_2-SAMs with different thicknesses, cyclic voltammograms of $Fc(CH_2OH)_2$ for different samples at pH 7 and 3, cyclic voltammograms of $Fe(CN)_6^{3-}$ for different samples at different pH values, cyclic voltammograms of L-AA and $Fc(CH_2OH)_2$ upon SAM displacement for PS-*hν*-PEO (8k−2k)-derived nanoporous films, and surface free energies of the substrates (PDF)

AUTHOR INFORMATION

Corresponding Authors

Takashi Ito − *Department of Chemistry, Kansas State University, Manhattan, Kansas 66506-0401, United States;* orcid.org/0000-0001-7443-3157; Phone: 785-532-1451; Email: ito@ksu.edu

Yi Yi − *Department of Chemistry, Indiana University, Bloomington, Indiana 47405, United States*; Phone: 812-855-1324; Email: yiyi@indiana.edu

Authors

Herman Coceancigh − *Department of Chemistry, Kansas State University, Manhattan, Kansas 66506-0401, United States*

Jay N. Sharma − *Department of Chemistry, Kansas State University, Manhattan, Kansas 66506-0401, United States*

Fred C. Parks − *Department of Chemistry, Indiana University, Bloomington, Indiana 47405, United States*

Amar H. Flood − *Department of Chemistry, Indiana University, Bloomington, Indiana 47405, United States;* orcid.org/0000-0002-2764-9155

Complete contact information is available at: https://pubs.acs.org/10.1021/acs.langmuir.0c01572

Notes

The authors declare no competing financial interest.

ACKNOWLEDGMENTS

This work is financially supported by the U.S. National Science Foundation (CHE-1709285 to T.I. and CHE-1709625 to A.H.F. and Y.Y.). In addition, Y.Y. acknowledges the Nanoscale Characterization Facility at the Indiana University for use of GPC. The authors thank Prof. Daniel A. Higgins (Kansas State University) for his help with contact angle measurements.

REFERENCES

(1) Bates, F. S.; Fredrickson, G. H. Block Copolymers—Designer Soft Materials. *Phys. Today* **1999**, *52*, 32−38.

(2) Bang, J.; Jeong, U.; Ryu, D. Y.; Russell, T. P.; Hawker, C. J. Block Copolymer Nanolithography: Translation of Molecular Level Control to Nanoscale Patterns. *Adv. Mater.* **2009**, *21*, 4769−4792.

(3) Bates, C. M.; Maher, M. J.; Janes, D. W.; Ellison, C. J.; Willson, C. G. Block Copolymer Lithography. *Macromolecules* **2014**, *47*, 2−12.

(4) Hailes, R. L. N.; Oliver, A. M.; Gwyther, J.; Whittell, G. R.; Manners, I. Polyferrocenylsilanes: Synthesis, Properties, and Applications. *Chem. Soc. Rev.* **2016**, *45*, 5358−5407.

(5) Cummins, C.; Ghoshal, T.; Holmes, J. D.; Morris, M. A. Strategies for Inorganic Incorporation Using Neat Block Copolymer Thin Films for Etch Mask Function and Nanotechnological Application. *Adv. Mater.* **2016**, *28*, 5586−5618.

(6) Liu, S. S. Y.; Ludwigs, S. Electrochemical Manipulation of Aligned Block Copolymer Templates. *Macromol. Rapid Commun.* **2020**, *41*, 1900485.

(7) Jackson, E. A.; Hillmyer, M. A. Nanoporous Membranes Derived from Block Copolymers: From Drug Delivery to Water Filtration. *ACS Nano* **2010**, *4*, 3548−3553.

(8) Ito, T. Block Copolymer-Derived Monolithic Polymer Films and Membranes Comprising Self-Organized Cylindrical Nanopores for Chemical Sensing and Separations. *Chem.—Asian J.* **2014**, *9*, 2708−2718.

(9) Werber, J. R.; Osuji, C. O.; Elimelech, M. Materials for Next-Generation Desalination and Water Purification Membranes. *Nat. Rev. Mater.* **2016**, *1*, 16018.

(10) Ito, T.; Ghimire, G. Electrochemical Applications of Microphase-Separated Block Copolymer Thin Films. *ChemElectroChem* **2018**, *5*, 2937−2953.

(11) Hillmyer, M. A. Nanoporous Materials from Block Copolymer Precursors. *Block Copolymers II*; Advances in Polymer Science; Springer, 2005; Vol. *190*, pp 137−181.

(12) Thurn-Albrecht, T.; Steiner, R.; DeRouchey, J.; Stafford, C. M.; Huang, E.; Bal, M.; Tuominen, M.; Hawker, C. J.; Russell, T. P. Nanoscopic Templates from Oriented Block Copolymer Films. *Adv. Mater.* **2000**, *12*, 787−791.

(13) Zalusky, A. S.; Olayo-Valles, R.; Taylor, C. J.; Hillmyer, M. A. Mesoporous Polystyrene Monoliths. *J. Am. Chem. Soc.* **2001**, *123*, 1519−1520.

(14) Mao, H.; Hillmyer, M. A. Nanoporous Polystyrene by Chemical Etching of Poly(ethylene oxide) from Ordered Block Copolymers. *Macromolecules* **2005**, *38*, 4038−4039.

(15) Ndoni, S.; Vigild, M. E.; Berg, R. H. Nanoporous Materials with Spherical and Gyroid Cavities Created by Quantitative Etching of Polydimethylsiloxane in Polystyrene-Polydimethylsiloxane Block Copolymers. *J. Am. Chem. Soc.* **2003**, *125*, 13366−13367.

(16) Zhang, M.; Yang, L.; Yurt, S.; Misner, M. J.; Chen, J.-T.; Coughlin, E. B.; Venkataraman, D.; Russell, T. P. Highly ordered Nanoporous Thin Films from Cleavable Polystyrene-block-Poly-(ethylene oxide). *Adv. Mater.* **2007**, *19*, 1571−1576.

(17) Ryu, J.-H.; Park, S.; Kim, B.; Klaikherd, A.; Russell, T. P.; Thayumanavan, S. Highly Ordered Gold Nanotubes Using Thiols at a Cleavable Block Copolymer Interface. *J. Am. Chem. Soc.* **2009**, *131*, 9870−9871.

(18) Kang, M.; Moon, B. Synthesis of Photocleavable Poly(styrene-block-ethylene oxide) and Its Self-Assembly into Nanoporous Thin Films. *Macromolecules* **2009**, *42*, 455−458.

(19) Schumers, J.-M.; Gohy, J.-F.; Fustin, C.-A. A Versatile Strategy for the Synthesis of block Copolymers Bearing a Photocleavable Junction. *Polym. Chem.* **2010**, *1*, 161−163.

(20) Zhao, H.; Gu, W.; Sterner, E.; Russell, T. P.; Coughlin, E. B.; Theato, P. Highly Ordered Nanoporous Thin Films from Photocleavable Block Copolymers. *Macromolecules* **2011**, *44*, 6433−6440.

(21) Schumers, J.-M.; Vlad, A.; Huynen, I.; Gohy, J.-F.; Fustin, C.-A. Functionalized Nanoporous Thin Films From Photocleavable Block Copolymers. *Macromol. Rapid Commun.* **2012**, *33*, 199−205.

(22) Gamys, C. G.; Schumers, J.-M.; Vlad, A.; Fustin, C.-A.; Gohy, J.-F. Amine-Functionalized Nanoporous Thin Films from a Poly-(ethylene oxide)-block-Polystyrene Diblock Copolymer Bearing a Photocleavable o-Nitrobenzyl Carbamate Junction. *Soft Matter* **2012**, *8*, 4486−4493.

(23) Zhao, H.; Gu, W.; Thielke, M. W.; Sterner, E.; Tsai, T.; Russell, T. P.; Coughlin, E. B.; Theato, P. Functionalized Nanoporous Thin Films and Fibers from Photocleavable Block Copolymers Featuring Activated Esters. *Macromolecules* **2013**, *46*, 5195−5201.

(24) Zhao, H.; Gu, W.; Kakuchi, R.; Sun, Z.; Sterner, E.; Russell, T. P.; Coughlin, E. B.; Theato, P. Photocleavable Triblock Copolymers Featuring an Activated Ester Middle Block: "One-Step" Synthesis and Application as Locally Reactive Nanoporous Thin Films. *ACS Macro Lett.* **2013**, *2*, 966−969.

(25) Wang, H. S.; Kim, K. H.; Bang, J. Thermal Approaches to Perpendicular Block Copolymer Microdomains in Thin Films: A Review and Appraisal. *Macromol. Rapid Commun.* **2019**, *40*, 1800728.

(26) Kim, G.; Libera, M. Morphological Development in Solvent-Cast Polystyrene−Polybutadiene−Polystyrene (SBS) Triblock Copolymer Thin Films. *Macromolecules* **1998**, *31*, 2569−2577.
(27) Sinturel, C.; Vayer, M.; Morris, M.; Hillmyer, M. A. Solvent Vapor Annealing of Block Polymer Thin Films. *Macromolecules* **2013**, *46*, 5399−5415.
(28) Brassat, K.; Lindner, J. K. N. Nanoscale Block Copolymer Self-Assembly and Microscale Polymer Film Dewetting: Progress in Understanding the Role of Interfacial Energies in the Formation of Hierarchical Nanostructures. *Adv. Mater. Interfaces* **2020**, *7*, 1901565.
(29) Pickett, G. T.; Witten, T. A.; Nagel, S. R. Equilibrium Surface Orientation of Lamellae. *Macromolecules* **1993**, *26*, 3194−3199.
(30) Huang, E.; Russell, T. P.; Harrison, C.; Chaikin, P. M.; Register, R. A.; Hawker, C. J.; Mays, J. Using Surface Active Random Copolymers to Control the Domain Orientation in Diblock Copolymer Thin Films. *Macromolecules* **1998**, *31*, 7641−7650.
(31) Niemz, A.; Bandyopadhyay, K.; Tan, E.; Cha, K.; Baker, S. M. Fabrication of Nanoporous Templates from Diblock Copolymer Thin Films on Alkylchlorosilane-Neutralized Surfaces. *Langmuir* **2006**, *22*, 11092−11096.
(32) Thurn-Albrecht, T.; Schotter, J.; Kastle, G. A.; Emley, N.; Shibauchi, T.; Krusin-Elbaum, L.; Guarini, K.; Black, C. T.; Tuominen, M. T.; Russell, T. P. Ultrahigh-Density Nanowire Arrays Grown in Self-Assembled Diblock Copolymer Templates. *Science* **2000**, *290*, 2126−2129.
(33) Jeoung, E.; Galow, T. H.; Schotter, J.; Bal, M.; Ursache, A.; Tuominen, M. T.; Stafford, C. M.; Russell, T. P.; Rotello, V. M. Fabrication and Characterization of Nanoelectrode Arrays Formed via Block Copolymer Self-Assembly. *Langmuir* **2001**, *17*, 6396−6398.
(34) Hirota, K.; Tajima, K.; Hashimoto, K. Facile Preparation of Nanoelectrode Ensembles Using Amphiphilic Block Copolymer Film. *Langmuir* **2005**, *21*, 11592−11595.
(35) Maire, H. C.; Ibrahim, S.; Li, Y.; Ito, T. Effects of Substrate Roughness on the Orientation of Cylindrical Domains in Thin Films of a Polystyrene-Poly(Methylmethacrylate) Diblock Copolymer Studied Using Atomic Force Microscopy and Cyclic Voltammetry. *Polymer* **2009**, *50*, 2273−2280.
(36) Genzer, J.; Kramer, E. J. Wetting of Substrates with Phase-Separated Binary Polymer Mixtures. *Phys. Rev. Lett.* **1997**, *78*, 4946−4949.
(37) Heier, J.; Kramer, E. J.; Walheim, S.; Krausch, G. Thin Diblock Copolymer Films on Chemically Heterogeneous Surfaces. *Macromolecules* **1997**, *30*, 6610−6614.
(38) Kim, T.; Chan, K. C.; Crooks, R. M. Polymeric Self-Assembled Monolayers. 4. Chemical, Electrochemical, and Thermal Stability of ω-Functionalized, Self-Assembled Diacetylenic and Polydiacetylenic Monolayers. *J. Am. Chem. Soc.* **1997**, *119*, 189−193.
(39) Love, J. C.; Estroff, L. A.; Kriebel, J. K.; Nuzzo, R. G.; Whitesides, G. M. Self-Assembled Monolayers of Thiolates on Metals as a Form of Nanotechnology. *Chem. Rev.* **2005**, *105*, 1103−1170.
(40) Kim, S. H.; Misner, M. J.; Xu, T.; Kimura, M.; Russell, T. P. Highly Oriented and Ordered Arrays from Block Copolymers via Solvent Evaporation. *Adv. Mater.* **2004**, *16*, 226−231.
(41) Bang, J.; Kim, B. J.; Stein, G. E.; Russell, T. P.; Li, X.; Wang, J.; Kramer, E. J.; Hawker, C. J. Effect of Humidity on the Ordering of PEO-Based Copolymer Thin Films. *Macromolecules* **2007**, *40*, 7019−7025.
(42) Kim, T. H.; Hwang, J.; Hwang, W. S.; Huh, J.; Kim, H.-C.; Kim, S. H.; Hong, J. M.; Thomas, E. L.; Park, C. Hierarchical Ordering of Block Copolymer Nanostructures by Solvent Annealing Combined with Controlled Dewetting. *Adv. Mater.* **2008**, *20*, 522−527.
(43) Kim, T. H.; Park, Y. J.; Song, G.; Kim, D. H.; Huh, J.; Karthaus, O.; Park, C. Micropatterns of Non-Circular Droplets of Nanostructured PS-b-PEO Copolymer by Solvent-Assisted Wetting on a Chemically Periodic Surface. *Macromol. Chem. Phys.* **2012**, *213*, 431−438.
(44) Cheng, Q.; Brajter-Toth, A. Selectivity and Sensitivity of Self-Assembled Thioctic Acid Electrodes. *Anal. Chem.* **1992**, *64*, 1998−2000.
(45) Wirde, M.; Gelius, U.; Nyholm, L. Self-Assembled Monolayers of Cystamine and Cysteamine on Gold Studied by XPS and Voltammetry. *Langmuir* **1999**, *15*, 6370−6378.
(46) Raj, C. R.; Ohsaka, T. Analytical Applications of Functionalized Self-Assembled Monolayers on Gold Electrode: Voltammetric Sensing of DOPAC at the Physiological Level. *Electroanalysis* **2002**, *14*, 679−684.
(47) Li, Y.; Ito, T. Size-Exclusion Properties of Nanoporous Films Derived from Polystyrene-Poly(methylmethacrylate) Diblock Copolymers Assessed Using Direct Electrochemistry of Ferritin. *Anal. Chem.* **2009**, *81*, 851−855.
(48) Pandey, B.; Tran Ba, K. H.; Li, Y.; Diaz, R.; Ito, T. Electrochemical Study of the Diffusion of Cytochrome c within Nanoscale Pores Derived from Cylinder-Forming Polystyrene-Poly-(methylmethacrylate) Diblock Copolymers. *Electrochim. Acta* **2011**, *56*, 10185−10190.
(49) Harandizadeh, Z.; Ito, T. Block Copolymer-Derived Recessed Nanodisk-Array Electrodes as Platforms for Folding-Based Electrochemical DNA Sensors. *ChemElectroChem* **2019**, *6*, 5627−5632.
(50) Li, Y.; Maire, H. C.; Ito, T. Electrochemical Characterization of Nanoporous Films Fabricated from a Polystyrene-Poly-(methylmethacrylate) Diblock Copolymer: Monitoring the Removal of the PMMA Domains and Exploring the Functional Groups on the Nanopore Surface. *Langmuir* **2007**, *23*, 12771−12776.
(51) Baker, L. A.; Jin, P.; Martin, C. R. Biomaterials and Biotechnologies Based on Nanotube Membranes. *Crit. Rev. Solid State Mater. Sci.* **2005**, *30*, 183−205.
(52) Yan, F.; Lin, X.; Su, B. Vertically Ordered Silica Mesochannel Films: Electrochemistry and Analytical Applications. *Analyst* **2016**, *141*, 3482−3495.
(53) Walcarius, A. Silica-Based Electrochemical Sensors and Biosensors: Recent Trends. *Curr. Opin. Electrochem.* **2018**, *10*, 88−97.
(54) Giri, D.; Hanks, C. N.; Collinson, M. M.; Higgins, D. A. Single-Molecule Spectroscopic Imaging Studies of Polarity Gradients Prepared by Infusion-Withdrawal Dip-Coating. *J. Phys. Chem. C* **2014**, *118*, 6423−6432.
(55) Trasatti, S.; Petrii, O. A. Real Surface Area Measurements in Electrochemistry. *J. Electroanal. Chem.* **1992**, *327*, 353−376.
(56) Widrig, C. A.; Chung, C.; Porter, M. D. The Electrochemical Desorption of n-Alkanethiol Monolayers from Polycrystalline Au and Ag Electrodes. *J. Electroanal. Chem.* **1991**, *310*, 335−359.
(57) Ito, T. Ion-Channel-Mimetic Sensor for Trivalent Cations Based on Self-Assembled Monolayers of Thiol-Derivatized 4-Acyl-5-Pyrazolones on Gold. *J. Electroanal. Chem.* **2001**, *495*, 87−97.
(58) Il'ichev, Y. V.; Schwörer, M. A.; Wirz, J. Photochemical Reaction Mechanisms of 2-Nitrobenzyl Compounds: Methyl Ethers and Caged ATP. *J. Am. Chem. Soc.* **2004**, *126*, 4581−4595.
(59) Xu, J.; Hong, S. W.; Gu, W.; Lee, K. Y.; Kuo, D. S.; Xiao, S.; Russell, T. P. Fabrication of Silicon Oxide Nanodots with an Areal Density Beyond 1 Teradots Inch−2. *Adv. Mater.* **2011**, *23*, 5755−5761.
(60) Zhu, L.; Cheng, S. Z. D.; Calhoun, B. H.; Ge, Q.; Quirk, R. P.; Thomas, E. L.; Hsiao, B. S.; Yeh, F.; Lotz, B. Phase Structures and Morphologies Determined by Self-Organization, Vitrification, and Crystallization: Confined Crystallization in an Ordered Lamellar Phase of PEO-b-PS Diblock Copolymer. *Polymer* **2001**, *42*, 5829−5839.
(61) Wu, S. *Polymer Interface and Adhesion*; Marcel Dekker: New York, 1982; pp 178−181.
(62) Ito, T.; Namba, M.; Bühlmann, P.; Umezawa, Y. Modification of Silicon Nitride Tips with Trichlorosilane Self-Assembled Monolayers (SAMs) for Chemical Force Microscopy. *Langmuir* **1997**, *13*, 4323−4332.
(63) Miyazawa, T.; Fukushima, K.; Ideguchi, Y. Molecular Vibrations and Structure of High Polymers. III. Polarized Infrared Spectra, Normal Vibrations, and Helical Conformation of Polyethylene Glycol. *J. Chem. Phys.* **1962**, *37*, 2764−2776.

https://dx.doi.org/10.1021/acs.langmuir.0c01572
Langmuir 2020, 36, 9259−9268

(64) Li, Y.; Ito, T. Surface Chemical Functionalization of Cylindrical Nanopores Derived from a Polystyrene−Poly(methylmethacrylate) Diblock Copolymer via Amidation. *Langmuir* **2008**, *24*, 8959−8963.
(65) Arrigan, D. W. M. Nanoelectrodes, Nanoelectrode Arrays and their Applications. *Analyst* **2004**, *129*, 1157−1165.
(66) Zoski, C. G.; Wijesinghe, M. Electrochemistry at Ultramicroelectrode Arrays and Nanoelectrode Ensembles of Macro- and Ultramicroelectrode Dimensions. *Isr. J. Chem.* **2010**, *50*, 347−359.
(67) Tran Ba, K. H.; Ito, T. Finite-Element Computer Simulations on Cyclic Voltammograms Measured at Recessed Nanodisk-Array Electrodes. *ECS Trans.* **2013**, *45*, 89−95.
(68) Albert, J. N. L.; Young, W.-S.; Lewis, R. L., III; Bogart, T. D.; Smith, J. R.; Epps, T. H., III Systematic Study on the Effect of Solvent Removal Rate on the Morphology of Solvent Vapor Annealed ABA Triblock Copolymer Thin Films. *ACS Nano* **2012**, *6*, 459−466.
(69) Helfand, E.; Tagami, Y. Theory of the Interface between Immiscible Polymers. *J. Polym. Sci., Part B: Polym. Lett.* **1971**, *9*, 741−746.
(70) Yuan, R.; Teran, A. A.; Gurevitch, I.; Mullin, S. A.; Wanakule, N. S.; Balsara, N. P. Ionic Conductivity of Low Molecular Weight Block Copolymer Electrolytes. *Macromolecules* **2013**, *46*, 914−921.
(71) Altinpinar, S.; Zhao, H.; Ali, W.; Kappes, R. S.; Schuchardt, P.; Salehi, S.; Santoro, G.; Theato, P.; Roth, S. V.; Gutmann, J. S. Distortion of Ultrathin Photocleavable Block Copolymer Films during Photocleavage and Nanopore Formation. *Langmuir* **2015**, *31*, 8947−8952.

https://dx.doi.org/10.1021/acs.langmuir.0c01572
Langmuir 2020, 36, 9259−9268